

Open charm yields in d+Au collisions at $\sqrt{s_{NN}} = 200$ GeV

J. Adams,³ M.M. Aggarwal,²⁹ Z. Ahammed,⁴³ J. Amonett,²⁰ B.D. Anderson,²⁰ D. Arkhipkin,¹³ G.S. Averichev,¹² Y. Bai,²⁷ J. Balewski,¹⁷ O. Barannikova,³² L.S. Barnby,³ J. Baudot,¹⁸ S. Bekele,²⁸ V.V. Belaga,¹² R. Bellwied,⁴⁶ J. Berger,¹⁴ B.I. Bezverkhny,⁴⁸ S. Bharadwaj,³³ V.S. Bhatia,²⁹ H. Bichsel,⁴⁵ A. Billmeier,⁴⁶ L.C. Bland,⁴ C.O. Blyth,³ B.E. Bonner,³⁴ M. Botje,²⁷ A. Boucham,³⁸ A. Brandin,²⁵ A. Bravar,⁴ M. Bystersky,¹¹ R.V. Cadman,¹ X.Z. Cai,³⁷ H. Caines,⁴⁸ M. Calderón de la Barca Sánchez,⁴ J. Carroll,²¹ J. Castillo,²¹ D. Cebra,⁷ Z. Chajecki,⁴⁴ P. Chaloupka,¹¹ S. Chatopadhyay,⁴³ H.F. Chen,³⁶ Y. Chen,⁸ J. Cheng,⁴¹ M. Cherney,¹⁰ A. Chikianian,⁴⁸ W. Christie,⁴ J.P. Coffin,¹⁸ T.M. Cormier,⁴⁶ J.G. Cramer,⁴⁵ H.J. Crawford,⁶ D. Das,⁴³ S. Das,⁴³ M.M. de Moura,³⁵ A.A. Derevschikov,³¹ L. Didenko,⁴ T. Dietel,¹⁴ W.J. Dong,⁸ X. Dong,³⁶ J.E. Draper,⁷ F. Du,⁴⁸ A.K. Dubey,¹⁵ V.B. Dunin,¹² J.C. Dunlop,⁴ M.R. Dutta Mazumdar,⁴³ V. Eckardt,²³ W.R. Edwards,²¹ L.G. Efimov,¹² V. Emelianov,²⁵ J. Engelage,⁶ G. Eppley,³⁴ B. Erazmus,³⁸ M. Estienne,³⁸ P. Fachini,⁴ J. Faivre,¹⁸ R. Fatemi,¹⁷ J. Fedorisin,¹² K. Filimonov,²¹ P. Filip,¹¹ E. Finch,⁴⁸ V. Fine,⁴ Y. Fisyak,⁴ K.J. Foley,⁴ K. Fomenko,¹² J. Fu,⁴¹ C.A. Gagliardi,³⁹ J. Gans,⁴⁸ M.S. Ganti,⁴³ L. Gaudichet,³⁸ F. Geurts,³⁴ V. Ghazikhanian,⁸ P. Ghosh,⁴³ J.E. Gonzalez,⁸ O. Grachov,⁴⁶ O. Grebenyuk,²⁷ D. Grosnick,⁴² S.M. Guertin,⁸ Y. Guo,⁴⁶ A. Gupta,¹⁹ T.D. Gutierrez,⁷ T.J. Hallman,⁴ A. Hamed,⁴⁶ D. Hardtke,²¹ J.W. Harris,⁴⁸ M. Heinz,² T.W. Henry,³⁹ S. Hepplemann,³⁰ B. Hippolyte,⁴⁸ A. Hirsch,³² E. Hjort,²¹ G.W. Hoffmann,⁴⁰ H.Z. Huang,⁸ S.L. Huang,³⁶ E.W. Hughes,⁵ T.J. Humanic,²⁸ G. Igo,⁸ A. Ishihara,⁴⁰ P. Jacobs,²¹ W.W. Jacobs,¹⁷ M. Janik,⁴⁴ H. Jiang,⁸ P.G. Jones,³ E.G. Judd,⁶ S. Kabana,² K. Kang,⁴¹ M. Kaplan,⁹ D. Keane,²⁰ V.Yu. Khodyrev,³¹ J. Kiryluk,²² A. Kisiel,⁴⁴ E.M. Kislov,¹² J. Klay,²¹ S.R. Klein,²¹ A. Klyachko,¹⁷ D.D. Koetke,⁴² T. Kollegger,¹⁴ M. Kopytine,²⁰ L. Kotchenda,²⁵ M. Kramer,²⁶ P. Kravtsov,²⁵ V.I. Kravtsov,³¹ K. Krueger,¹ C. Kuhn,¹⁸ A.I. Kulikov,¹² A. Kumar,²⁹ C.L. Kunz,⁹ R.Kh. Kutuev,¹³ A.A. Kuznetsov,¹² M.A.C. Lamont,³ J.M. Landgraf,⁴ S. Lange,¹⁴ F. Laue,⁴ J. Lauret,⁴ A. Lebedev,⁴ R. Lednický,¹² S. Lehocká,¹² M.J. LeVine,⁴ C. Li,³⁶ Q. Li,⁴⁶ Y. Li,⁴¹ S.J. Lindenbaum,²⁶ M.A. Lisa,²⁸ F. Liu,⁴⁷ L. Liu,⁴⁷ Q.J. Liu,⁴⁵ Z. Liu,⁴⁷ T. Ljubicic,⁴ W.J. Llope,³⁴ H. Long,⁸ R.S. Longacre,⁴ M. Lopez-Noriega,²⁸ W.A. Love,⁴ Y. Lu,⁴⁷ T. Ludlam,⁴ D. Lynn,⁴ G.L. Ma,³⁷ J.G. Ma,⁸ Y.G. Ma,³⁷ D. Magestro,²⁸ S. Mahajan,¹⁹ D.P. Mahapatra,¹⁵ R. Majka,⁴⁸ L.K. Mangotra,¹⁹ R. Manweiler,⁴² S. Margetis,²⁰ C. Markert,⁴⁸ L. Martin,³⁸ J.N. Marx,²¹ H.S. Matis,²¹ Yu.A. Matulenko,³¹ C.J. McClain,¹ T.S. McShane,¹⁰ F. Meissner,²¹ Yu. Melnick,³¹ A. Meschanin,³¹ M.L. Miller,²² Z. Milosevich,⁹ N.G. Minaev,³¹ C. Mironov,²⁰ A. Mischke,²⁷ D. Mishra,¹⁵ J. Mitchell,³⁴ B. Mohanty,⁴³ L. Molnar,³² C.F. Moore,⁴⁰ M.J. Mora-Corral,²³ D.A. Morozov,³¹ V. Morozov,²¹ M.G. Munhoz,³⁵ B.K. Nandi,⁴³ T.K. Nayak,⁴³ J.M. Nelson,³ P.K. Netrakanti,⁴³ V.A. Nikitin,¹³ L.V. Nogach,³¹ B. Norman,²⁰ S.B. Nurushev,³¹ G. Odyniec,²¹ A. Ogawa,⁴ V. Okorokov,²⁵ M. Oldenburg,²¹ D. Olson,²¹ S.K. Pal,⁴³ Y. Panebratsev,¹² S.Y. Panitkin,⁴ A.I. Pavlinov,⁴⁶ T. Pawlak,⁴⁴ T. Peitzmann,²⁷ V. Perevozchikov,⁴ C. Perkins,⁶ W. Peryt,⁴⁴ V.A. Petrov,¹³ S.C. Phatak,¹⁵ R. Picha,⁷ M. Planinic,⁴⁹ J. Pluta,⁴⁴ N. Porile,³² J. Porter,⁴ A.M. Poskanzer,²¹ M. Potekhin,⁴ E. Potrebenikova,¹² B.V.K.S. Potukuchi,¹⁹ D. Prindle,⁴⁵ C. Pruneau,⁴⁶ J. Putschke,²³ G. Rai,²¹ G. Rakness,³⁰ R. Raniwala,³³ S. Raniwala,³³ O. Ravel,³⁸ R.L. Ray,⁴⁰ S.V. Razin,¹² D. Reichhold,³² J.G. Reid,⁴⁵ G. Renault,³⁸ F. Retiere,²¹ A. Ridiger,²⁵ H.G. Ritter,²¹ J.B. Roberts,³⁴ O.V. Rogachevskiy,¹² J.L. Romero,⁷ A. Rose,⁴⁶ C. Roy,³⁸ L. Ruan,³⁶ I. Sakrejda,²¹ S. Salur,⁴⁸ J. Sandweiss,⁴⁸ I. Savin,¹³ P.S. Sazhin,¹² J. Schambach,⁴⁰ R.P. Scharenberg,³² N. Schmitz,²³ L.S. Schroeder,²¹ K. Schweda,²¹ J. Seger,¹⁰ P. Seyboth,²³ E. Shahaliev,¹² M. Shao,³⁶ W. Shao,⁵ M. Sharma,²⁹ W.Q. Shen,³⁷ K.E. Shestermanov,³¹ S.S. Shimanskiy,¹² F. Simon,²³ R.N. Singaraju,⁴³ G. Skoro,¹² N. Smirnov,⁴⁸ R. Snellings,²⁷ G. Sood,⁴² P. Sorensen,²¹ J. Sowinski,¹⁷ J. Speltz,¹⁸ H.M. Spinka,¹ B. Srivastava,³² A. Stadnik,¹² T.D.S. Stanislaus,⁴² R. Stock,¹⁴ A. Stolpovsky,⁴⁶ M. Strikhanov,²⁵ B. Stringfellow,³² A.A.P. Suade,³⁵ E. Sugarbaker,²⁸ C. Suire,⁴ M. Sumbera,¹¹ B. Surrow,²² T.J.M. Symons,²¹ A. Szanto de Toledo,³⁵ P. Szarwas,⁴⁴ A. Tai,⁸ J. Takahashi,³⁵ A.H. Tang,²⁷ T. Tarnowsky,³² D. Thein,⁸ J.H. Thomas,²¹ S. Timoshenko,²⁵ M. Tokarev,¹² T.A. Trainor,⁴⁵ S. Trentalange,⁸ R.E. Tribble,³⁹ O. Tsai,⁸ J. Ulery,³² T. Ullrich,⁴ D.G. Underwood,¹ A. Urkinbaev,¹² G. Van Buren,⁴ M. van Leeuwen,²¹ A.M. Vander Molen,²⁴ R. Varma,¹⁶ I.M. Vasilevski,¹³ A.N. Vasiliev,³¹ R. Vernet,¹⁸ S.E. Vigdor,¹⁷ V.P. Viyogi,⁴³ S. Vokal,¹² S.A. Voloshin,⁴⁶ M. Vznuzdaev,²⁵ B. Waggner,¹⁰ F. Wang,³² G. Wang,²⁰ G. Wang,⁵ X.L. Wang,³⁶ Y. Wang,⁴⁰ Y. Wang,⁴¹ Z.M. Wang,³⁶ H. Ward,⁴⁰ J.W. Watson,²⁰ J.C. Webb,¹⁷ R. Wells,²⁸ G.D. Westfall,²⁴ A. Wetzler,²¹

C. Whitten Jr.,⁸ H. Wieman,²¹ S.W. Wissink,¹⁷ R. Witt,² J. Wood,⁸ J. Wu,³⁶ N. Xu,²¹ Z. Xu,⁴ Z.Z. Xu,³⁶ E. Yamamoto,²¹ P. Yepes,³⁴ V.I. Yurevich,¹² Y.V. Zanevsky,¹² H. Zhang,⁴ W.M. Zhang,²⁰ Z.P. Zhang,³⁶ P.A. Zolnierczuk,¹⁷ R. Zoukarneev,¹³ Y. Zoukarneeva,¹³ and A.N. Zubarev¹²
(STAR Collaboration)

¹Argonne National Laboratory, Argonne, Illinois 60439

²University of Bern, Bern, Switzerland CH-3012

³University of Birmingham, Birmingham, United Kingdom

⁴Brookhaven National Laboratory, Upton, New York 11973

⁵California Institute of Technology, Pasadena, California 91125

⁶University of California, Berkeley, California 94720

⁷University of California, Davis, California 95616

⁸University of California, Los Angeles, California 90095

⁹Carnegie Mellon University, Pittsburgh, Pennsylvania 15213

¹⁰Creighton University, Omaha, Nebraska 68178

¹¹Nuclear Physics Institute AS CR, 250 68 Řež/Prague, Czech Republic

¹²Laboratory for High Energy (JINR), Dubna, Russia

¹³Particle Physics Laboratory (JINR), Dubna, Russia

¹⁴University of Frankfurt, Frankfurt, Germany

¹⁵Insitute of Physics, Bhubaneswar 751005, India

¹⁶Indian Institute of Technology, Mumbai, India

¹⁷Indiana University, Bloomington, Indiana 47408

¹⁸Institut de Recherches Subatomiques, Strasbourg, France

¹⁹University of Jammu, Jammu 180001, India

²⁰Kent State University, Kent, Ohio 44242

²¹Lawrence Berkeley National Laboratory, Berkeley, California 94720

²²Massachusetts Institute of Technology, Cambridge, MA 02139-4307

²³Max-Planck-Institut für Physik, Munich, Germany

²⁴Michigan State University, East Lansing, Michigan 48824

²⁵Moscow Engineering Physics Institute, Moscow Russia

²⁶City College of New York, New York City, New York 10031

²⁷NIKHEF, Amsterdam, The Netherlands

²⁸Ohio State University, Columbus, Ohio 43210

²⁹Panjab University, Chandigarh 160014, India

³⁰Pennsylvania State University, University Park, Pennsylvania 16802

³¹Institute of High Energy Physics, Protvino, Russia

³²Purdue University, West Lafayette, Indiana 47907

³³University of Rajasthan, Jaipur 302004, India

³⁴Rice University, Houston, Texas 77251

³⁵Universidade de São Paulo, São Paulo, Brazil

³⁶University of Science & Technology of China, Anhui 230027, China

³⁷Shanghai Institute of Applied Physics, Shanghai 201800, P.R. China

³⁸SUBATECH, Nantes, France

³⁹Texas A&M University, College Station, Texas 77843

⁴⁰University of Texas, Austin, Texas 78712

⁴¹Tsinghua University, Beijing, P.R. China

⁴²Valparaiso University, Valparaiso, Indiana 46383

⁴³Variable Energy Cyclotron Centre, Kolkata 700064, India

⁴⁴Warsaw University of Technology, Warsaw, Poland

⁴⁵University of Washington, Seattle, Washington 98195

⁴⁶Wayne State University, Detroit, Michigan 48201

⁴⁷Institute of Particle Physics, CCNU (HZNU), Wuhan, 430079 China

⁴⁸Yale University, New Haven, Connecticut 06520

⁴⁹University of Zagreb, Zagreb, HR-10002, Croatia

(Dated: March 22, 2019)

Open charm spectra at mid-rapidity from direct reconstruction of $D^0(\overline{D^0}) \rightarrow K^\mp\pi^\pm$ in d+Au collisions and indirect electron/positron measurements via charm semileptonic decays in p+p and d+Au collisions at $\sqrt{s_{NN}} = 200$ GeV are reported. The $D^0(\overline{D^0})$ spectrum covers a transverse momentum (p_T) range of $0.1 < p_T < 3$ GeV/c whereas the electron spectra cover a range of $1 < p_T < 4$ GeV/c. The electron spectra show approximately binary collision scaling between p+p and d+Au collisions. From these two independent analyses, the differential cross section per nucleon-nucleon interaction

at mid-rapidity for open charm production from d+Au collisions at RHIC is $d\sigma_{c\bar{c}}^{NN}/dy = 0.30 \pm 0.04$ (stat.) ± 0.09 (syst.) mb. Next-to-leading-order pQCD calculations underpredict the charm yield. Consequences for A+A collisions at RHIC from this large yield are discussed.

PACS numbers: 25.75.Dw, 13.20.Fc, 13.20.Ft, 24.85.+p Version 2.0

Hadrons with heavy flavors are unique tools for studying strong interactions which are described by Quantum Chromodynamics (QCD). Due to their large quark masses, which require large energies ($\gtrsim 3$ GeV) for their creation, their production is sensitive to initial conditions and their spectra are sensitive to the later stage dynamical evolution in high energy nuclear collisions. The charm cross section is expected to be less affected by the non-perturbative complications in theoretical calculations [1, 2]. Charm production has been proposed as a sensitive measurement of the parton distribution function in the nucleon, and the nuclear shadowing effect, by systematic studies of p+p, and p+nucleus collisions [3]. The predicted reduced energy loss of heavy quarks should allow one to study the energy loss mechanism within the partonic medium [4].

A possible enhancement of charmonium (J/ψ) production can be present at RHIC energies [5, 6, 7] through charm quark coalescence. This effect is the opposite of the possible J/ψ suppression in a Quark-Gluon Plasma (QGP) in the absence of that process [8]. The measurement of both the open charm and charmonium yields may allow us to quantify the effects and study the chemical equilibrium of the system. In addition, the heavy flavor transverse momentum distributions and their anisotropic flow can be used to study early thermalization in A+A collisions. This is possible since the frequent rescatterings that would be necessary for the heavy-quark collective motion may result in the equilibration of light quarks.

Identification of charmed hadrons is difficult due to their short lifetime ($c\tau(D^0) = 124 \mu\text{m}$), low production rates, and large combinatoric background. Most measurements of the total charm cross section in hadron-hadron collisions were performed at low center-of-mass energies ($\lesssim 40$ GeV) in fixed target experiments [9, 10]. At $\sqrt{s} \sim 52 - 63$ GeV, the available measurements are not conclusive due to inconsistencies between different measurements [9, 11]. The measurements at higher energy colliders were either at high p_T only [12], or with large uncertainties [13, 14]. Theoretical predictions for the RHIC energy region differ significantly [15, 16]. Therefore, precise measurements of charm cross sections in p+p and d+Au collisions in this energy region are crucial.

In this paper, we report the first results on the open charm cross section measurements from direct charmed hadron $D^0(\overline{D}^0)$ reconstruction in d+Au

collisions, and electrons from charm semileptonic decay in both p+p and d+Au collisions at $\sqrt{s_{\text{NN}}} = 200$ GeV. Both methods are complementary and provide important cross checks.

The data used in D^0 direct reconstruction and charm semileptonic decay analysis were taken during the 2003 RHIC run in d+Au and p+p collisions at $\sqrt{s_{\text{NN}}} = 200$ GeV with the Solenoidal Tracker at RHIC (STAR). A minimum bias d+Au collision trigger was defined by requiring at least one spectator neutron in the Au beam outgoing direction depositing energy in the Zero Degree Calorimeter (ZDC). Detailed descriptions of the trigger and centrality definition in d+Au collisions have been presented in the previous publication [17]. A total of 15.7 million minimum bias triggered d+Au collision events were used in the D^0 analysis. The data samples used in the electron analysis in d+Au and p+p collisions were described in Ref. [18]. The integrated luminosity is about $40 \mu\text{b}^{-1}$ for d+Au collisions and 30 nb^{-1} for p+p collisions.

The primary tracking device of the STAR detector is the Time Projection Chamber (TPC) [19] which was used to reconstruct the decay of $D^0 \rightarrow K^-\pi^+$ ($\overline{D}^0 \rightarrow K^+\pi^-$) which has a branching ratio of 3.83%. In what follows, we imply $(D^0 + \overline{D}^0)/2$ when using the term D^0 unless otherwise specified. The exact D^0 decay topology cannot be resolved due to insufficient track projection resolution close to the collision vertex. The invariant mass spectrum of D^0 was obtained by pairing each oppositely charged kaon and pion candidates in the same event. The kaon and pion tracks were identified through the ionization energy loss (dE/dx) in the TPC wherever the identification is possible. Candidate tracks were selected with their momenta $p(p_T) > 0.3(0.2)$ GeV/c, and pseudorapidity $|\eta| < 1$. The D^0 signal with $p_T < 3$ GeV/c and $|y| < 1$ after mixed-event background subtraction [20] is shown in the left panel of Fig. 1. The signal-to-background ratio (S/N) is about 1/600, and the figure of merit (S/\sqrt{N}) is about 6. In addition to the D^0 signal, there remains residual background, which may be due to di-hadron correlation from jets, cannot be described by the mixed-event spectrum. This distribution was fit to a Gaussian plus a linear function. The open symbols in the left panel of Fig. 1 depict the D^0 signal after the two-step background subtraction. Within statistical uncertainties, the yields of D^0 and \overline{D}^0 are equal. The $D^0 \rightarrow K^-\pi^+$ signal could

be mis-identified as a $\overline{D^0} \rightarrow K^+ \pi^-$ and vice versa when both of its daughters' momenta are beyond particle identification in the TPC. This misidentification results in double counting and was corrected for in the D^0 yields through a Monte Carlo simulation.

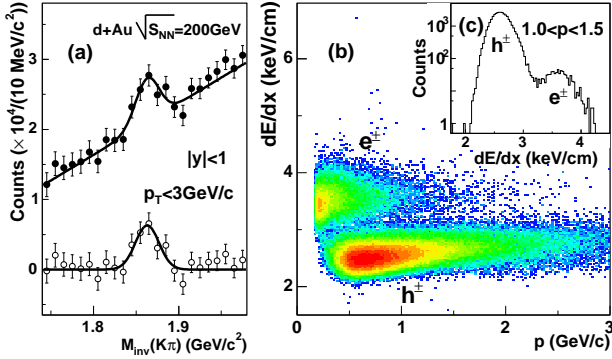


FIG. 1: (a) Invariant mass distributions of kaon-pion pairs from d+Au collisions. The solid circles depict the signal after mixed-event background subtraction, the open circles after subtraction of the residual background using a linear parametrization. (b) dE/dx in the TPC vs. particle momentum (p) with a TOF cut of $|1/\beta - 1| \leq 0.03$. Insert: The projection of the dE/dx for $1 < p < 1.5$ GeV/c.

A prototype time-of-flight system (TOFr) [21] based on the multi-gap resistive plate chamber technology was installed in STAR. It covers azimuthal angle $\Delta\phi \simeq \pi/30$, $-1 < \eta < 0$, and allows particle identification for $p_T < 3.5$ GeV/c. In addition to its capability of hadron identification [18], electrons/positrons could be identified at low momentum ($p_T < 3$ GeV/c) by the combination of velocity (β) from TOFr and dE/dx from TPC measurements. The right panel of Fig. 1 demonstrates the clean separation of electrons from hadrons using their dE/dx in the TPC after applying a TOFr cut of $|1/\beta - 1| \leq 0.03$. This cut eliminated the hadrons crossing the electron dE/dx band. Electrons/positrons were required to originate from the collision vertex. At higher p_T (2–4 GeV/c), electrons were identified directly in the TPC since hadrons have lower dE/dx due to the relativistic rise of the dE/dx for electrons. Positrons are more difficult to identify using dE/dx alone because of the large background from the deuteron band. The correction for hadron contamination was evaluated to be 5–30%, depending on p_T . Detector acceptance and efficiency corrections were determined from detailed simulations [18]. Total inclusive electron spectra from 200 GeV p+p and d+Au collisions are shown in Fig. 2.

Gamma conversions $\gamma \rightarrow e^+e^-$ and $\pi^0 \rightarrow \gamma e^+e^-$ Dalitz decays are the dominant photonic sources of

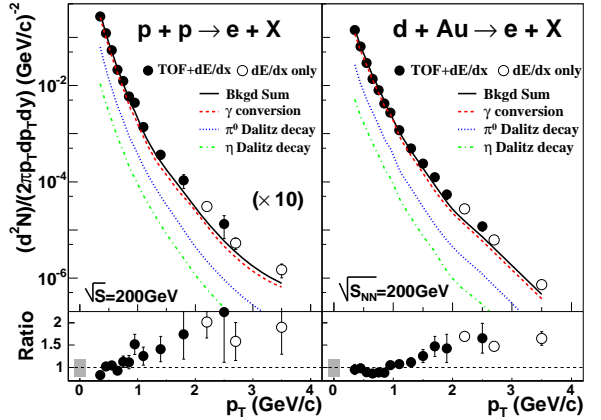


FIG. 2: Upper panels: Electron distributions from p+p (left $\times 10$) and d+Au (right) collisions. Solid and open symbols depict electrons/positrons $((e^+ + e^-)/2)$ identified via a combination of Time-of-Flight (TOF) and dE/dx , and electrons (e^-) identified via dE/dx alone. The total photonic backgrounds are shown as solid lines. Dashed lines depict the various contributing sources. The fractions were derived from simulations. Bottom panels: Ratios of inclusive electrons over the total backgrounds. The gray bands represent the systematic uncertainties.

electron background. To measure the background photonic electron spectra, the invariant mass and opening angle of the e^+e^- pairs were constructed from an electron (positron) in TOFr and every positron (electron) candidate reconstructed in the TPC [22] without the additional requirement of a secondary vertex at the conversion point. Simulations with both HIJING [23] and PYTHIA [24] with full detector description in GEANT yielded a $\sim 60\%$ efficiency for electrons with $p_T > 1$ GeV/c from such background processes. More than 95% of the electrons from sources other than charm semileptonic decays have been measured with this method, while the remaining fraction ($< 5\%$) from decays of η, ω, ρ, ϕ and K was determined from simulations. The results are shown as solid lines in Fig. 2. The overall uncertainty of the background is on the order of 20% and was included in the systematic errors. Ratios of the inclusive electrons over the total backgrounds are shown in the bottom panels of Fig. 2. Clear signal excesses are visible with $p_T > 1$ GeV/c.

The non-photonic electron spectra were obtained by subtracting the previously described photonic background from the inclusive spectra. The results are shown in Fig. 3. The D^0 invariant yields $d^2N/2\pi p_T dp_T dy$ as a function of p_T are shown in Fig. 3 as solid squares. The yield dN/dy for D^0 at midrapidity was extracted using an exponential fit to the differential yield in transverse mass (m_T) [20],

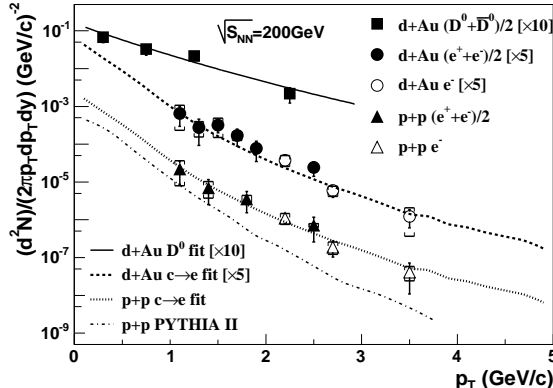


FIG. 3: Reconstructed D^0 (solid squares) p_T distributions from d+Au collisions. Non-photonic electron p_T distributions from p+p collisions (triangles) and d+Au collisions (circles). Solid and dashed lines are the fit results from both D^0 and electron spectra in d+Au collisions. The dotted line is scaled down by a factor of $N_{bin} = 7.5 \pm 0.4$ [17] from d+Au to p+p collisions. The dot-dashed line is from PYTHIA II calculation [24].

and listed in the first row in Table I. We performed a fit with the combined results of D^0 and electron distributions in d+Au collisions, assuming that the D^0 spectrum follows a power law in p_T and that the remaining electrons after background subtraction are from charm semileptonic decays [1, 24]. The results are depicted in Fig. 3. The yield difference between the two fitting methods is much smaller than the statistical uncertainty. The systematic error is dominated by the uncertainties in the background subtraction, the extrapolation due to finite p_T coverage, and the overall normalization ($\pm 14\%$ in p+p and $\pm 10\%$ in d+Au collisions [17, 18]).

The yield of D^0 at mid-rapidity is $dN/dy = 0.028 \pm 0.004 \pm 0.008$ and the $\langle p_T \rangle = 1.32 \pm 0.08$ GeV/c in the d+Au collisions. We used the ratio $R = N_{D^0}/N_{c\bar{c}} = 0.54 \pm 0.05$ from e^+e^- collider [25] to convert the D^0 yield to total $c\bar{c}$ yield. A p+p inelastic scattering cross section of $\sigma_{inel}^{pp} = 42 \text{ mb}$ was used in the calculation and a factor of $f = 4.7 \pm 0.7$, estimated from simulations [15, 24], was used to convert the $d\sigma/dy$ at mid-rapidity to the total cross section. The total charm cross section per nucleon-nucleon interaction for d+Au collisions at 200 GeV is $\sigma_{c\bar{c}}^{NN} = dN_{D^0}^{d+Au}/dy \times \sigma_{inel}^{pp}/N_{bin}^{d+Au} \times f/R = 1.3 \pm 0.2 \pm 0.4 \text{ mb}$ from D^0 alone and $1.4 \pm 0.2 \pm 0.4 \text{ mb}$ from the combined fit of D^0 and electrons. The nuclear modification factor [17] was obtained by taking the ratio of the electron spectra in d+Au and p+p collisions scaled with the underlying nucleon-nucleon binary collisions. It was measured to be $1.3 \pm 0.3 \pm 0.3$ averaging over $1 < p_T < 4 \text{ GeV}/c$ and is consistent

with binary scaling within the measured errors.

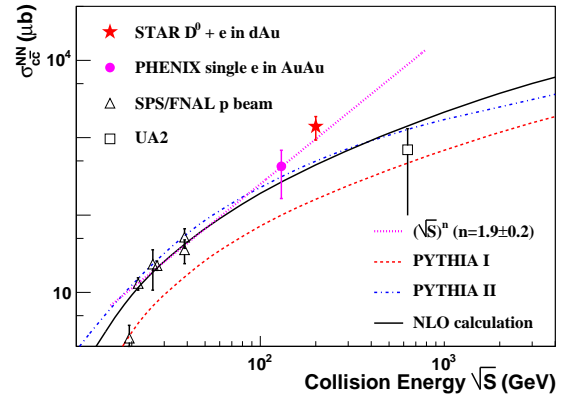


FIG. 4: Total $c\bar{c}$ cross section per nucleon-nucleon collision vs. the collision energy ($\sqrt{s_{NN}}$). The result of this measurement is depicted by a star. The dotted-line is a power-law fit. Dashed- and dot-dashed-lines are PYTHIA calculations with different options [24]. The solid line is a NLO pQCD calculation from [15].

	$dN(D^0)/dy _{y=0} (10^{-2})$	$d\sigma_{c\bar{c}}^{NN}/dy _{y=0} (\text{mb})$
D^0	$2.8 \pm 0.4 \pm 0.8$	$0.29 \pm 0.04 \pm 0.08$
$D^0 + e^\pm$	$2.9 \pm 0.4 \pm 0.8$	$0.30 \pm 0.04 \pm 0.09$

TABLE I: dN/dy of D^0 in d+Au collisions and the corresponding $d\sigma/dy$ of $c\bar{c}$ pair per nucleon-nucleon collision at $\sqrt{s_{NN}} = 200 \text{ GeV}$. A fraction of $N_{D^0}/N_{c\bar{c}} = 0.54 \pm 0.05$ and a pp inelastic collision cross section of 42 mb at $\sqrt{s_{NN}} = 200 \text{ GeV}$ were used for the calculation.

The beam energy dependence of the cross section is shown in Fig. 4. The cross sections reported by UA2 in $\sqrt{s} = 630 \text{ GeV}$ p+ \bar{p} collisions and PHENIX in $\sqrt{s_{NN}} = 130 \text{ GeV}$ Au+Au collisions were derived from the measurements of single electrons from charm semileptonic decays [13, 14]. The dotted line is a power law fit of $\sigma_{c\bar{c}}^{NN} \propto (\sqrt{s})^n$ to the data points, with $n = 1.9 \pm 0.2$, while $n \sim 0.3$ (0.5) had been observed for charged hadrons (pions) productions in central Au+Au collisions [5, 26, 27, 28] and the inclusive hadron production in p+p collisions has a $\ln(s)$ dependence [29]. This indicates a harder behavior of the underlying process going from charged hadron production to charm dominated processes. This power-law dependence of the hadron production at high energy hadron-hadron collisions is related to the x -dependence of the gluon distribution function. The dashed and dot-dashed lines depict PYTHIA calculations with and without higher order processes, such as flavor excitation. The solid line depicts the next-to-leading order (NLO) pQCD calculation from [15]. At $\sqrt{s_{NN}} = 200 \text{ GeV}$, both

PYTHIA and NLO pQCD calculations underpredict the total charm cross section by at least a factor of 3. This is also evident from the comparison of the electron p_T distributions in Fig. 3. In addition, the slope from PYTHIA simulations is steeper than that of the data. There are also indications that a large charm production cross section ($\sigma_{cc}^{NN} \simeq 2-3$ mb) at $\sqrt{s_{NN}} \simeq 300$ GeV is essential to explain the cosmic ray data [28].

Since charm quarks are massive and only expected to be created through hard QCD processes [3], charm production in heavy ion collisions should scale with the number of binary interactions. This implies a large charm yield in Au+Au collisions at RHIC. Statistical thermal models [5, 6, 7] predicted an enhancement of J/ψ in Au+Au collisions via the coalescence of charm and anti-charm quarks. Our measurement scaled by binary collisions to central Au+Au collisions indicates that about a factor of 3 enhancement of J/ψ yield above binary scaling would be expected from coalescence of charm quarks in a thermalized system without additional absorption effects [5, 6, 7]. The upper limit (below binary scaling) from the PHENIX Collaboration on J/ψ production in central Au+Au collisions invalidates this expectation [30]. Future heavy ion runs at RHIC with open charm and J/ψ measurements will enable us to study the flow and thermalization

of charmed particles.

In summary, charm cross section and transverse momentum distributions from p+p and d+Au collisions at $\sqrt{s_{NN}} = 200$ GeV have been measured by the STAR collaboration at RHIC. The independent measurements of the reconstructed D^0 and single electrons from charm semileptonic decay are consistent. The NLO calculation underpredicts the total cross section at this energy. The combination of the large open charm cross section in elementary collisions and the upper limit on J/ψ production below binary scaling in central Au+Au collisions rules out the expectation of J/ψ enhancement from some charm coalescence models.

We are grateful for many fruitful discussions with D. Kharzeev, and R. Vogt. We thank the RHIC Operations Group and RCF at BNL, and the NERSC Center at LBNL for their support. This work was supported in part by the HENP Divisions of the Office of Science of the U.S. DOE; the U.S. NSF; the BMBF of Germany; IN2P3, RA, RPL, and EMN of France; EPSRC of the United Kingdom; FAPESP of Brazil; the Russian Ministry of Science and Technology; the Ministry of Education and the NNSFC of China; Grant Agency of the Czech Republic, FOM and UU of the Netherlands, DAE, DST, and CSIR of the Government of India; Swiss NSF; and the Polish State Committee for Scientific Research.

[1] P.L. McGaughey *et al.*, *Int. J. Mod. Phys. A* **10**, 2999 (1995).
[2] S.S. Adler *et al.*, (PHENIX Collaboration), *Phys. Rev. Lett.* **91**, 241803 (2003); J. Adams *et al.*, (STAR Collaboration), *Phys. Rev. Lett.* **92**, 171801 (2004).
[3] Z. Lin and M. Gyulassy, *Phys. Rev. Lett.* **77**, 1222 (1996).
[4] Y.L. Dokshitzer and D.E. Kharzeev, *Phys. Lett. B* **519**, 199 (2001).
[5] A. Andronic *et al.*, *Phys. Lett. B* **571**, 36 (2003), and references therein.
[6] R.L. Thews, M. Schroedter, and J. Rafelski, *Phys. Rev. C* **63**, 054905 (2001), and references therein.
[7] M.I. Gorenstein *et al.*, *J. Phys. G* **28**, 2151 (2002).
[8] T. Matsui and H. Satz, *Phys. Lett. B* **178**, 416 (1986).
[9] S.P.K. Tavernier, *Rep. Prog. Phys.* **50**, 1439 (1987) and references therein.
[10] G.A. Alves *et al.*, (E769 Collaboration), *Phys. Rev. Lett.* **77**, 2388 (1996).
[11] F.W. Büsser *et al.*, *Nucl. Phys. B* **113**, 189 (1976).
[12] D. Acosta *et al.*, (CDF II Collaboration), *Phys. Rev. Lett.* **91**, 241804 (2003).
[13] K. Adcox *et al.*, (PHENIX Collaboration), *Phys. Rev. Lett.* **88**, 192303 (2002).
[14] O. Botner *et al.*, *Phys. Lett. B* **236**, 488 (1990).
[15] R. Vogt, hep-ph/0203151, and references therein. The curve in Fig. 4 is a NLO pQCD calculation with CTEQ5M, $\mu_F = \mu_R = 2m_c$, $m_c = 1.2$ GeV/ c^2 .
[16] J. Raufeisen and J.-C. Peng, *Phys. Rev. D* **67**, 054008 (2003).
[17] J. Adams *et al.*, (STAR Collaboration), *Phys. Rev. Lett.* **91**, 072304 (2003).
[18] J. Adams *et al.*, (STAR Collaboration), submitted to *Phys. Rev. Lett.*, Sept. 2003 nucl-ex/0309012.
[19] M. Anderson *et al.*, *Nucl. Instr. Meth. A* **499**, 659 (2003).
[20] C. Adler *et al.*, *Phys. Rev. C* **66**, 061901(R)(2002); H. Zhang, *J. Phys. G* **30**, S577 (2004); H. Zhang, Ph.D. thesis, Yale University, 2003.
[21] B. Bonner *et al.*, *Nucl. Instr. Meth. A* **508**, 181 (2003); M. Shao *et al.*, *Nucl. Instr. Meth. A* **492**, 344 (2002).
[22] J. Adams *et al.*, (STAR Collaboration), submitted to *Phys. Rev. C*, (2004); nucl-ex/0401008; I. Johnson, Ph.D. thesis, U.C. Davis, 2002.
[23] X.N. Wang and M. Gyulassy, *Phys. Rev. D* **44**, 3501 (1991).
[24] T. Sjöstrand *et al.*, *Computer Physics Commun.* **135**, 238 (2001). In this paper we used PYTHIA 6.152 with the parameter settings I: MSEL=4, CTEQ5M1 and II: MSEL=1, CTEQ5M1.
[25] K. Hagiwara *et al.*, *Phys. Rev. D* **66**, 010001 (2002)

(Particle Data Group).

- [26] D. Kharzeev and E. Levin, *Phys. Lett. B* **523**, 79 (2001). D. Kharzeev and K. Tuchin, *Nucl. Phys. A* **735**, 248 (2004).
- [27] S.V. Afanasiev *et al.*, (NA49 Collaboration), *Phys. Rev. C* **66**, 054902 (2002).
- [28] I.V. Rakobolskaya *et al.*, *Nucl. Phys. B* **122**, 353 (2003) (Proc. Suppl.).
- [29] F. Abe *et al.*, *Phys. Rev. D* **41**, 2330R (1990).
- [30] S.S. Adler *et al.*, (PHENIX Collaboration), *Phys. Rev. C* **69**, 014901 (2004); S.S. Adler *et al.*, (PHENIX Collaboration), *Phys. Rev. Lett.* **92**, 051802 (2004).